Applied Catalysis B: Environmental 96 (2010) 101–109

Contents lists available at ScienceDirect

Applied Catalysis B: Environmental

journal homepage: www.elsevier.com/locate/apcatb

Effects of adsorbed and gaseous NO_x species on catalytic oxidation of diesel soot with MnO_x–CeO_2 mixed oxides

Xiaodong Wu *, Fan Lin, Haibo Xu, Duan Weng

Laboratory of Advanced Materials, Department of Materials Science and Engineering, Tsinghua University, Beijing 100084, China

ARTICLE INFO

Article history:
Received 9 October 2009
Received in revised form 3 February 2010
Accepted 4 February 2010
Available online 10 February 2010

Keywords:
MnOx–CeO_2 mixed oxides
Soot oxidation
NO oxidation
Nitrate storage
Surface oxygen complexes

ABSTRACT

MnO_x–CeO_2, MnO_x and CeO_2 catalysts were synthesized by the sol–gel method. The structural, redox and adsorption properties of the individual and mixed oxides were investigated by X-ray diffraction (XRD), Brunauer–Emmett–Teller (BET), CO temperature-programmed reduction (TPR), NO temperature-programmed oxidation (TPO), NO_x temperature-programmed desorption (TPD) and *in situ* diffuse reflectance infrared Fourier transform spectroscopy (DRIFTS). The TPO tests were performed with the soot–catalyst mixture under loose contact conditions to evaluate the catalytic activity of the oxide catalysts for soot oxidation. The MnO_x–CeO_2 mixed oxide catalyst presents the lowest soot oxidation temperature among the catalysts investigated in the presence of NO and O_2. The synergetic effect between manganese oxide and ceria restrains the growth of oxide crystallites, increases the specific surface area and improves the low-temperature redox property. Especially, the activity of MnO_x–CeO_2 mixed oxides for NO oxidation and its capacity for NO_2 storage in the form of surface nitrates are greatly enhanced. Not only the NO_2 released from decomposition of surface nitrates but also that formed by catalytic oxidation of gaseous or adsorbed NO on the catalyst is confirmed important for soot oxidation. It is found by the *in situ* DRIFTS tests with the soot–catalyst mixture that the generation of surface oxygen complexes (SOCs), such as carboxylic anhydrides, lactones, quinine, ceto-enol groups, ethers and phenols, occurs at about 100 °C lower temperature with exposure to NO than in the absence of NO, which is an important step for soot oxidation.

1. Introduction

In the past decades, the high fuel efficiency, reliability and durability of diesel engines have led to the dominance in commercial vehicles and an unprecedented growth of their share in the passenger car market. Nitrogen oxides and particulate matter emission are two important pollutants in the exhaust from diesel engines [1]. The use of a catalytic trap performing both filtration and catalytic combustion of soot appears to be a promising solution for soot removal [2].

To develop suitable catalysts capable of promoting soot oxidation by NO_x is an efficient way for removal of diesel soot at low temperatures and has been exploited in Johnson Matthey's continuously regeneration technology (CRT) [3]. This reduction mostly involves NO_2 molecules by direct reaction with soot to form NO and, to a much less extent, N_2 and N_2O [4,5]. Lots of perovskite- and spinel-type oxides have been reported to be effective catalysts for NO_x-assisted soot oxidation [2,6–8]. Platinum-based catalysts, providing NO to NO_2 oxidation, exhibit high activity in spite of their expensive costs [9–11]. Recently, transition metals such as manganese, copper and cobalt based catalysts show strong soot oxidation activity because of their strong oxidative property [12–18]. Ceria has been used as an oxygen storage material for three-way catalysts and been proven to be as an effective component of soot oxidation catalysts [19–22]. The strong oxidative property of transition metals in combination with the oxygen storage property of ceria makes transition metal–ceria mixed oxide catalysts as one group of cheap and efficient candidate catalysts for soot oxidation. Tikhomirov et al. [23] have found that the MnO_x–CeO_2 mixed oxides with the Mn:Ce ratio of 1:3 exhibit a superior activity for NO-assisted soot oxidation, which can be traced its ability to store NO at low temperature in form of nitrates followed by a release of NO_2 as a strong oxidizing agent at high temperatures. However, the contributions of nitrate- and NO-derived NO_2 are not distinguished in their work.

In the present study, the potential of MnO_x–CeO_2 mixed oxides in acceleration of NO_2-soot reaction was further examined in respect to the individual oxide catalysts. The importance of

* Corresponding author. Tel.: +86 10 62792375; fax: +86 10 62792375.
E-mail address: wuxiaodong@tsinghua.edu.cn (X. Wu).

0926-3373/$ – see front matter © 2010 Elsevier B.V. All rights reserved.
doi:10.1016/j.apcatb.2010.02.006

nitrate- and NO-derived NO_2 species, which were released from decomposition of surface nitrates and formed by catalytic oxidation of gaseous NO, respectively, was demonstrated for soot oxidation on the catalysts. Especially, the *in situ* DRIFTS tests with the soot–catalyst mixture were carried out in the presence of $NO + O_2$ and O_2, respectively, to explore possible intermediates generated on the surface of soot.

2. Experimental

2.1. Catalyst preparation

The MnO_x–CeO_2 mixed oxide catalyst was prepared by the sol–gel method. The nitrates $Ce(NO_3)_3{\cdot}6H_2O$ (99.0 wt.%, Beijing Yili) and $Mn(NO_3)_2$ (50% water solution, Yili) were mixed in deionized water according to the molar ratio of Mn:Ce = 15:85. The citric acid was added dropwise as the complexing agent with a 1.3:1 ratio of the acid to metal ions including Ce^{3+} and Mn^{2+}. Appropriate polyglycol was followed with the weight of 10% citric acid added. The blended solution was sufficiently mixed in a magnetic stirrer and heated at 80 °C till the transparent gel was formed. The resulting gel was dried at 110 °C overnight. The received powders were submitted to decomposition at 300 °C for 1 h and calcination at 500 °C for 3 h under static air in a muffle. The powders were cooled to room temperature (RT) in the furnace to obtain MnO_x–CeO_2 mixed oxides. The individual oxides CeO_2 and MnO_x were prepared by a similar method.

2.2. Catalyst characterization

The powder X-ray diffraction (XRD) experiments were determined by a Japan Science D/max-RB diffractometer employing Cu Kα radiation (λ = 0.15418 nm). The X-ray tube was operated at 40 kV and 120 mA. The X-ray powder diffractograms were recorded at 0.02° intervals in the range of $20^\circ \leq 2\theta \leq 80^\circ$ with a scanning velocity of 6°/min.

The bulk compositions of the mixed oxide catalysts were examined by X-ray fluorescence (XRF) spectroscopy using a Shimadzu XRF-1800 instrument.

The specific surface areas of the samples were measured using the N_2 adsorption isotherm at −196 °C by the five-point Brunauer–Emmett–Teller (BET) method using an automatic surface analyzer (Quantachrome NOVA 4000). The samples were degassed in flowing N_2 at 200 °C for 2 h.

The CO temperature-programmed reduction (TPR) tests were performed in a fixed-bed reactor with the effluent gases monitored by a mass spectrometer (OmniStar 200). Prior to the test, 50 mg of the sample was treated with O_2 (2 vol%)/He (50 ml/min) at 500 °C for 30 min, and was then cooled down to RT in the same atmosphere. It was subsequently flushed by He (50 ml/min) for 30 min to remove the physisorbed molecules. Finally, the reactor temperature was raised up to 800 °C at a heating rate of 10 °C/min in CO (4 vol%)/He (75 ml/min).

The NO temperature-programmed oxidation (TPO) tests were carried out in a fixed-bed reactor with the effluent gases monitored by an infrared spectrometer (Thermo Nicolet 380). The gas mixture of 1200 ppm NO/10% O_2/N_2 was fed to 100 mg of the sample at a flow rate of 500 ml/min. The reactor temperature was ramped to 550 °C at a heating rate of 10 °C/min.

The NO_x temperature-programmed desorption (TPD) tests were performed in the same apparatus. Prior to the test, 500 mg of the powder sample was placed in a tubular quartz reactor (i.d. = 10 mm) and was treated in 10% O_2/N_2 at 500 °C for 30 min. After the NO_x adsorption in 1000 ppm NO/10% O_2/N_2 at 350 °C for 30 min and subsequent cooling to RT, the desorption profiles of NO_2 and NO were obtained by ramping the reactor to 500 °C at a heating rate of 10 °C/min in a N_2 stream (50 ml/min).

The diffuse reflectance infrared Fourier transform spectra (DRIFTS) were recorded on a Nicolet 6700 spectrometer equipped with a temperature-controllable diffuse reflection chamber and a high sensitivity of MCT detector. The weight ratio of the catalyst to soot was 10:1, and that of the soot–catalyst mixture to KBr was 1:40. The mixed powders were purged *in situ* in a N_2 stream at 500 °C for 30 min, and were then cooled down to RT. The background spectrum was taken at each temperature. After then, a gas mixture of 10% O_2/N_2 or 1000 ppm NO/10% O_2/N_2 was fed at a flow rate of 50 ml/min. All the spectra were determined by accumulating 100 scans at a resolution of 4 cm^{-1} as a function of temperature at a heating rate of 10 °C/min or of adsorption time at 400 °C. Adsorption of NO_x on MnO_x–CeO_2 mixed oxides without soot was also investigated by the infrared spectroscopy.

2.3. Catalytic activity measurement

Printex-U (Degussa) was used as a model soot. Its particle size was 25 nm and the specific surface area was 100 m^2/g. The catalytic activities of the catalysts for soot oxidation were evaluated by a temperature-programmed oxidation (TPO) reaction apparatus. The soot and catalyst powders were mixed carefully in a 1/10 weight ratio by a spatula for "loose contact" conditions. In order to prevent reaction runaway, 110 mg of the soot–catalyst mixture was diluted with 300 mg of silica pellets. The diluted or undiluted mixture was placed in a tubular quartz reactor (i.d. = 10 mm), and the oxidation test was carried out in the temperature range from RT to 500 °C at a heating rate of 20 °C/min. The inlet gas mixture was 1000 ppm NO/10% O_2 or 10% O_2 in nitrogen with a flow rate of 500 ml/min. The concentrations of CO_2 and CO in the outlet gas mixture were determined on-line by a five-component analyzer FGA4015 with an infrared sensor. The temperature at which the CO_2 concentration reached 500 ppm and 5000 ppm in the outlet gas was referred to as the ignition temperature (T_i) of soot oxidation with the diluted and undiluted soot–catalyst mixture, respectively, which in general reflected the intrinsic characteristics of the catalytic material and was relatively difficult to be affected by reaction conditions. T_m represented the maximal soot oxidation rate temperature. The total molar ratio of $CO_2/(CO_2 + CO)$ in the outlet gas during soot oxidation process was defined as the selectivity to CO_2 (S_{CO_2}).

3. Results and discussion

3.1. XRD and BET

The bulk composition of the mixed oxides was determined by XRF. The molar ratio of Mn/(Mn + Ce) in the mixed oxides is found to be around 0.145, indicating that the MnO_x–CeO_2 sample presents the expected composition according to the applied sol–gel method. The powder XRD patterns of the mixed and individual oxides are shown in Fig. 1. MnO_x–CeO_2 mixed oxides present the characteristic peaks attributed to ceria with a cubic fluorite structure, and no manganese oxides are detected. Mn occurs mainly in +3 oxidation state with minor Mn_3O_4 phase in the MnO_x sample. Table 1 summarizes the lattice constants of ceria and manganese sesquioxide in the samples based on the XRD data from Cohen's method, as well as the mean crystallite sizes according to Debye–Scherrer equation.

The lattice constant of ceria decreases obviously with the doping of manganese, which indicates the incorporation of Mn cations into the ceria lattice due to the smaller ionic radii of Mn^{3+} (0.065 nm) and Mn^{2+} (0.083 nm) in comparison with those of Ce^{4+} (0.097 nm) and Ce^{3+} (0.114 nm) as well as their structural

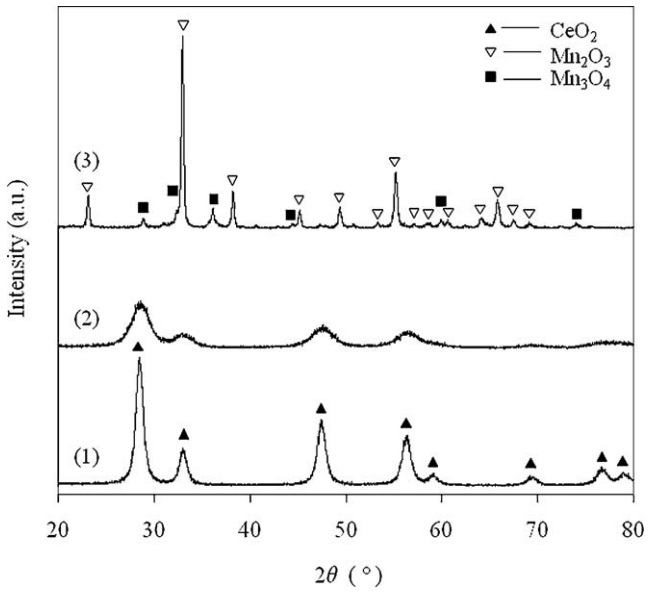

Fig. 1. XRD patterns of (1) CeO_2, (2) MnO_x–CeO_2 and (3) MnO_x.

similarity. It has been reported that the solubility of Mn in ceria depends strongly on how the material is prepared [24,25]. No MnO_x diffraction peaks are detected at the Mn/(Mn + Ce) ratio of 0.15 in this work. However, the possibility of existence of highly dispersed manganese oxides, which cannot be detected by the XRD technique [26], on the surface of MnO_x–CeO_2 solid solution crystallites may not be excluded.

The obtained diffraction peaks for the mixed oxides are much broader than those for the individual oxides. As shown in the table, the mean crystallite size of the mixed oxides is significantly smaller than those of the individual oxides, indicating the inhibition effect of Mn incorporation on the growth of ceria-based crystallites. It is in good accordance with the order of the BET surface area of the catalysts. MnO_x–CeO_2 in the form of solid solutions has the smallest crystallite size and the largest specific surface area among the samples prepared. On the other hand, the BET area of pure MnO_x is exceptionally small owing to severe sintering of Mn_2O_3 crystallites.

Table 1
Solid properties of the catalysts.

Sample	Lattice constant (nm)	Crystallite size (nm)	S_{BET} (m^2/g)
CeO_2	0.5417	8.7	63
MnO_x	0.9403	33.2	22
MnO_x–CeO_2	0.5406	3.5	96

3.2. Soot TPO

To explore the effect of two types of NO_2 species on soot oxidation with different catalysts, the TPO tests were carried out by feeding different feed gas compositions (1000 ppm NO/10% O_2/N_2 and 10% O_2/N_2). For comparison, the catalyst was also pretreated by exposure to NO + O_2 at 350 °C for 30 min prior to mixing with soot and silica for the TPO test in O_2. The runs were performed under loose contact conditions and high flow rate to simulate actual operating conditions in a diesel particulate catalytic trap. Fig. 2 shows the evolutions of outlet CO_2 during the TPO tests under different conditions with CeO_2, MnO_x and MnO_x–CeO_2, respectively. NO_x is found to promote the soot oxidation significantly on all the catalysts.

As shown in Fig. 2a, the T_m of CeO_2 obtained in the presence of NO is 472 °C, with a considerable shift to lower temperature by 81 °C in respect to that obtained in the absence of NO. The NO + O_2

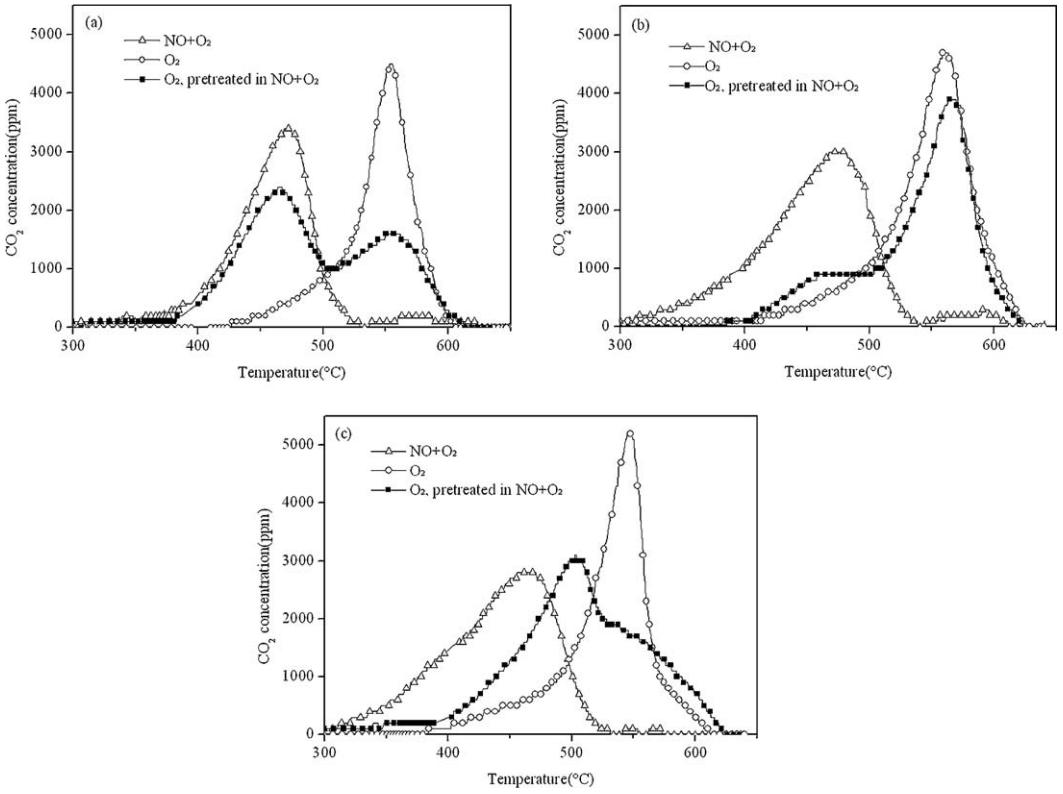

Fig. 2. TPO profiles of (a) CeO_2, (b) MnO_x and (c) MnO_x–CeO_2 in different atmospheres.

Table 2
Soot oxidation activities of the catalysts in NO + O_2.

Sample	Diluted soot–catalyst mixture			Undiluted soot–catalyst mixture		
	T_i (°C)	T_m (°C)	S_{CO_2} (%)	T_i (°C)	T_m (°C)	S_{CO_2} (%)
CeO_2	396	472	93	440	445	94
MnO_x	359	474	99	434	441	95
MnO_x–CeO_2	345	463	98	378	384	95
No catalyst	545	600	47	563	583	30

pretreatment also facilitates the soot oxidation. A bimodal shape of the TPO profile is observed for the NO + O_2 pretreated CeO_2, with the low-temperature and high-temperature peaks correlating well with those obtained in NO + O_2 and O_2, respectively. It is also noted that both the ignition temperatures of CeO_2 in NO_2 + O_2 and the pretreated catalyst in O_2 are around 400 °C and a NO rise is observed with the low-temperature peak in the latter case (not shown). Thus, it can be suggested that the nitrate-derived NO_2 significantly promotes the soot oxidation with CeO_2 although the NO_x storage capacity of ceria cannot meet the complete oxidation of soot.

A shift of T_m by 85 °C to lower temperature is also observed on MnO_x by introduction of NO as one of the reactant gases in Fig. 2b. The low-temperature peak of the NO + O_2 pretreated MnO_x in O_2 is weak although its temperature coincides with that obtained in NO+ O_2, implying a poor NO_x storage capacity of the manganese oxide. Furthermore, the ignition temperature of the catalyst in NO + O_2 is much lower than 400 °C. Thus, there should be another source of NO_2 which contributes to assisting soot oxidation. According to the following characterizations, the NO_2 formed by catalytic oxidation of gaseous NO with active oxygen from the catalyst should play a definitive role in the reaction of soot with MnO_x in NO + O_2.

The introduction of NO into the reactant gases brings on a shift of T_m by 82 °C and T_i by 98 °C to lower temperature for the mixed oxide catalyst. The TPO curve of the NO + O_2 pretreated MnO_x–CeO_2 is between those obtained in NO + O_2 and O_2. Thus, it is reasonable to assume that the superior behavior of the mixed oxide catalyst in the presence of NO is not only related to nitrate-derived NO_2 but also originate from NO-derived NO_2.

In order to further compare the NO_x-assisted soot oxidation activities of these oxide catalysts, the TPO tests were performed with the diluted and undiluted soot–catalyst mixtures. The obtained T_i, T_m and S_{CO_2} values for the catalysed and uncatalysed combustion of soot are listed in Table 2. These catalysts always yield high CO_2 selectivity, indicating that the partial oxidation of soot is no longer a significant reaction. Accordingly, Fig. 3 only shows the evolutions of CO_2 and NO during the soot oxidation process for the sake of clarity.

As shown in Fig. 3a, the curves of CO_2 production for the diluted soot–catalyst mixtures exhibit a bimodal shape which are related to different dominant oxidizing agents at different stages of soot oxidation. The small low-temperature peak corresponds to the ignition of soot by NO_2, while the soot oxidation with O_2 is dominating at high temperature, which will be discussed in Section 3.5. Although the position of the maximal soot oxidation rate temperature is fixed at ca. 470 °C, the ignition temperature of the catalyst follows the order of MnO_x–CeO_2 > MnO_x > CeO_2. The T_i of MnO_x–CeO_2 is as low as 345 °C. The predominance of the mixed oxide catalyst in soot oxidation activity demonstrates the importance of both adsorbed and gaseous NO_x species. An obvious oxidative adsorption of NO is observed at low temperatures centered at 300–350 °C for MnO_x–CeO_2 and MnO_x, while the decrease of the outlet NO concentration is quite small for CeO_2. The increase of NO with the ignition of soot oxidation is not as obvious as expected, implying a possibility of reduction of NO_2 by soot to N_2.

A reaction runaway may take place depending upon the technique used [27,28]. If the soot–catalyst is undiluted, for example, the mass and heat transfer limitations will turn to be predominant. As shown in Fig. 3b and Table 2, the sharp TPO profiles as well as the small gaps between the T_i and T_m values suggest the occurrence of the runaway phenomena. The runaway may cause a loss of some data points in the TPO curves. The stored nitrates seem to play an important role in NO_x-assisted oxidation of soot with MnO_x–CeO_2 under an energy transference controlled regime, which may be ascribed to the close contact of surface nitrates and soot particles. A distinct NO increase occurs simultaneously with the ignition of soot oxidation and the outlet NO reaches a maximum at the maximal soot oxidation rate temperature, implying the assistance of NO_2 for soot oxidation and accordingly the reduction of the nitrate-derived NO_2 to NO. The exothermic soot oxidation reaction, in turn, initiates the extensive oxidation of soot by oxygen and accelerates the further decomposition of nitrates to produce more NO_x. Both these contributions can be considered as NO_x-assisted soot oxidation. Oxygen is the major oxidant during the whole process. Both the nitrate- and NO-derived NO_2

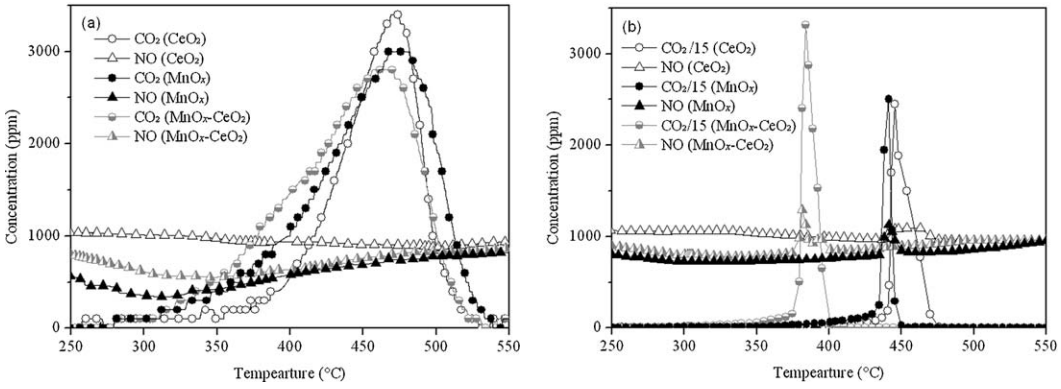

Fig. 3. TPO profiles of the (a) diluted and (b) undiluted soot–catalyst mixtures in NO + O_2.

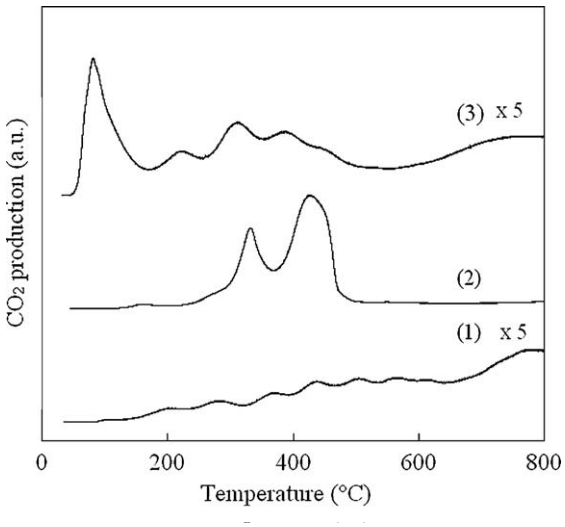

Fig. 4. CO-TPR profiles of (1) CeO_2, (2) MnO_x and (3) MnO_x–CeO_2.

only act as a ''trigger'' for the extensive oxidation of soot by oxygen.

3.3. CO-TPR

The CO-TPR tests were applied to evaluate the redox property of MnO_x–CeO_2 and individual oxides, and the results are shown in Fig. 4. Minor peaks are observed in the temperature range from 300 to 450 °C on ceria, which are always due to the reduction of surface oxygen species including hydroxyl groups, and the broad peak centered at 780 °C is ascribed to the reduction of lattice oxygen [29]. Two distinct peaks are found at 335 and 433 °C for pure MnO_x, which are related to the successive reductions of $Mn_2O_3 \rightarrow Mn_3O_4$ and $Mn_3O_4 \rightarrow MnO$, respectively.

Several reduction peaks are found around 83, 215, 307, 383 and 440 °C for MnO_x–CeO_2. The first one has a strong linkage with surface oxygen vacancies, which has been evidenced by the O_2-TPD test that a great amount of α-O_2 can be released from MnO_x–CeO_2 mixed oxides at low temperatures [30]. The formation of MnO_x–CeO_2 solid solutions has a positive effect on generation of surface oxygen vacancies from doping of low-valent Mn^{x+} (x = 2, 3) cations. It is also stressed that the strong interaction between Mn and Ce in the solid solutions significantly increases lattice oxygen lability of the mixed oxides. The peaks in the temperature range from 175 to 500 °C are assigned to the reduction of $Mn_2O_3 \rightarrow Mn_3O_4$, $Mn_3O_4 \rightarrow MnO$ and $Ce^{4+} \rightarrow Ce^{3+}$, respectively. In this way, active oxygen species can be readily generated on the surface of MnO_x–CeO_2 mixed oxides and facilitate both NO oxidation and soot oxidation at low temperatures.

3.4. NO-TPO and NO_x-TPD

It has been shown in Fig. 3 that the outlet NO decreases obviously at low temperatures after passing through MnO_x–CeO_2 and MnO_x during the soot-TPO test. In order to examine the catalytic activity of the catalysts for oxidation of NO to NO_2, the NO-TPO tests were carried out in a gas flow of 1200 ppm NO/10% O_2/N_2 and the results are shown in Fig. 5. Ceria shows a poor oxidation activity with 25% NO conversion in the temperature range from 420 to 500 °C in Fig. 5a, which correlates well with the NO evolution during soot-TPO test (Fig. 3). Comparatively, MnO_x exhibits an onset temperature at 95 °C and a maximal rate (70% NO conversion) temperature at 305 °C in Fig. 5b, revealing a remarkable activity for NO oxidation. It has been known from Fig. 4 that the reactivity of lattice oxygen is significantly higher in MnO_x–CeO_2 solid solutions than in the individual oxides. As a

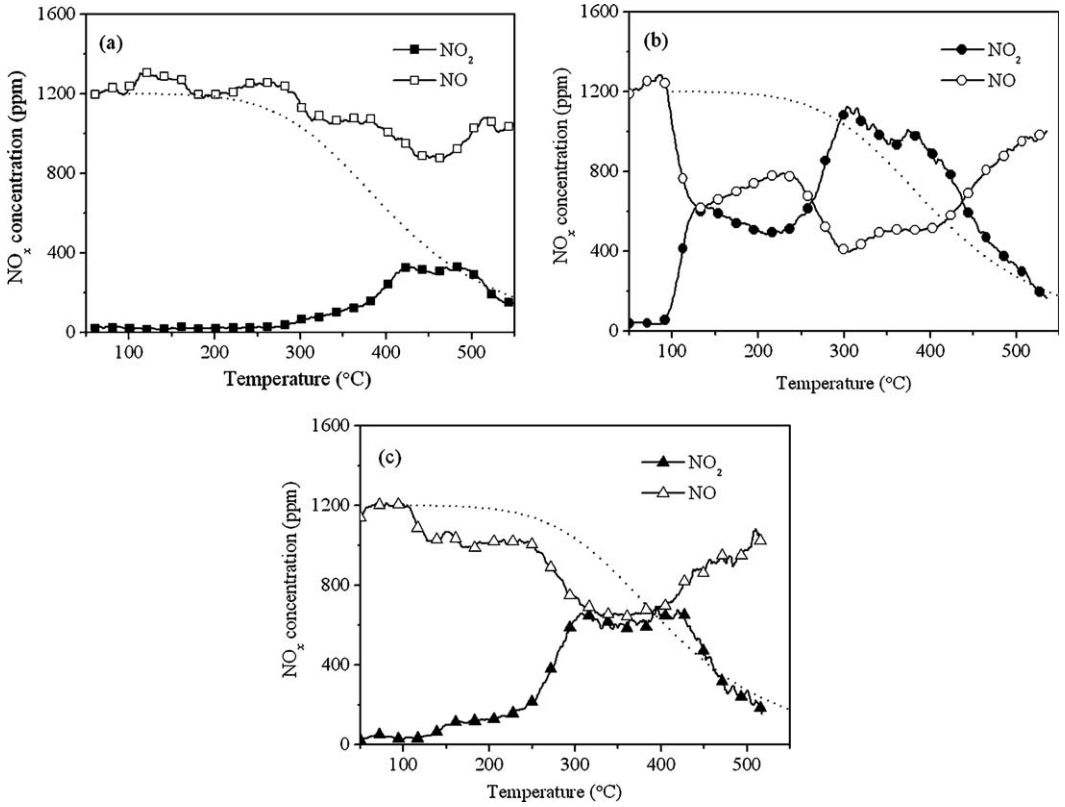

Fig. 5. NO-TPO profiles of (a) CeO_2, (b) MnO_x and (c) MnO_x–CeO_2.

result, the doping of Mn heavily enhances the ability of the mixed oxides for NO oxidation with a broad oxidation peak between 300 and 430 °C in Fig. 5c, which just lies in the temperature range where soot oxidation occurs with this catalyst.

The dotted line in the figures represents the NO_2 profile predicted by the thermodynamic equilibrium of the reaction $NO + (1/2)O_2 \leftrightarrow NO_2$. The importance of the catalysts especially MnO_x is highlighted at low temperatures at which NO_2 production is kinetically restricted. The limitation in NO_2 production is imposed by thermodynamics above a certain temperature. For this reason, the NO_2 profiles typically present a maximum NO_2 level. In Fig. 5a, the NO_2 concentration measured follows the values predicted by thermodynamics above 450 °C. On the contrary, it seems in Fig. 5b that the decomposition of chemisorbed NO_x species also contributes to the NO_2 level, which is slightly above the thermodynamically predicted values. The NO_2 production behavior of the MnO_x–CeO_2 mixed oxide in Fig. 5c is in between both situations.

Although the NO oxidation is remarkable on MnO_x, this catalyst shows a much poorer activity for soot oxidation than MnO_x–CeO_2 mixed oxides. The difference between the specific surface area of MnO_x and MnO_x–CeO_2 should be considered as an important fact for the solid-solid-gas reaction under loose contact conditions [31,32]. On the other hand, the adsorbed NO_x species on the catalyst surface, especially those stored as surface nitrates, are suggested to play an important role in the reaction. In order to evaluate the NO_x storage capacity of different catalysts, the NO_x desorption behaviors were investigated by means of TPD and the results are shown in Fig. 6. The catalysts were treated in a flow of 1000 ppm NO/10% O_2/N_2 at 350 °C prior to the TPD tests.

As shown in Fig. 6a, two NO_2 desorption peaks are observed at 200 and 290 °C on MnO_x–CeO_2, which are ascribed to decomposition of bidentate/monodentate nitrates and ionic nitrate, respectively. The first peak almost vanishes on CeO_2, while the ionic nitrate peak shifts to a higher temperature (370 °C). By contrast, no NO_2 desorption peaks are found on MnO_x. As shown in Fig. 6b, the distinct NO desorption peak at medium temperature (235, 355 and 420 °C for MnO_x, MnO_x–CeO_2 and CeO_2, respectively) may be attributed to the strongly bound nitrite species, while a weak shoulder at 150 °C may be ascribed to desorption of weakly adsorbed NO and/or decomposition of surface nitrites, which has been mostly outgassed by N_2 purging after the $NO + O_2$ adsorption. It is noted that the maximum of NO production lags just a few degrees above the maximum of a NO_2 peak. According to the following results determined by DRIFTS (Section 3.5), the adsorption of $NO + O_2$ on MnO_x–CeO_2 mixed oxides leads to the formation of nitrates as the major ad-NO_x species, whereas the adsorption of NO_x in the form of nitrites or molecular NO is not significant at medium temperatures. Thus, a more reasonable explanation is that the production of desorbed NO arises from the thermodynamic-driven decomposition of NO_2 and/or NO_2 dissociation on reducible metal sites during the TPD tests under N_2 [33]. This makes the interpretation of the desorption profiles complicated. The total amounts of NO_x (NO_2 + NO) stored on different catalysts were estimated from the desorption profiles. The amount of NO_x desorbed from MnO_x–CeO_2, CeO_2 and MnO_x is 0.533, 0.161 and 0.125 mmol/g, respectively. The NO_x species desorbed at low temperatures is thought to contribute little to the soot oxidation with MnO_x, and the readily decomposable nitrates at mild temperatures on CeO_2 may explain the soot oxidation activity comparable with MnO_x in despite of its relative weak redox property.

The weak basicity and small surface area account for the poor NO_x storage capacity of MnO_x. It is interesting not to find any NO_2 desorption peaks on MnO_x despite of its high NO oxidation ability. The catalyst with high NO oxidation ability and strong redox activity may release NO_2 ad-species preferentially as NO if the desorption is carried out under inert atmosphere, which is the case here. CeO_2 shows some nitrate storage capacity linked to its medium basicity and relatively high surface area despite its relative inefficiency for NO oxidation. The synergetic effect between Mn and Ce in solid solutions is believed to be responsible for the adsorption and activation of O_2 and NO molecules. The adsorbates as bidentate/monodentate and ionic nitrates are produced from oxidative adsorption of NO to NO_2 by lattice oxygens bound to Mn and subsequent coordination to Ce in adjacent surface sites [34]. Although this step is accompanied by the reduction of substituted Mn cations, the reoxidization should be easily accomplished by oxygen equilibration with the gas phase during the $NO + O_2$ coadsorption. Thus, the combination of high NO oxidation activity and high NO_2 storage capacity makes MnO_x–CeO_2 as an efficient catalyst for NO_x-assisted soot oxidation. It has been reported that MnO_x–CeO_2 catalysts even exceed the soot oxidation activity of a conversion Pt-based catalyst due to the additional contribution from desorption of NO_2 being stored at low temperatures [23].

3.5. In situ DRIFT

The DRIFT spectra of adsorbed species on MnO_x–CeO_2 were investigated to gain insight into the types of stored NO_x species. The N_2 flow containing 1000 ppm NO and 10% O_2 was introduced to the IR cell. The IR spectra were recorded every 100 °C at a heating rate of 10 °C/min, and the results are shown in Fig. 7a. Based on the obtained spectra and the previous reports [23,26,34–37], monodentate nitrates (1510, 1290 and 1040 cm^{-1}) and bidentate nitrates (1580, 1310 and 1040 cm^{-1}) are the main species at

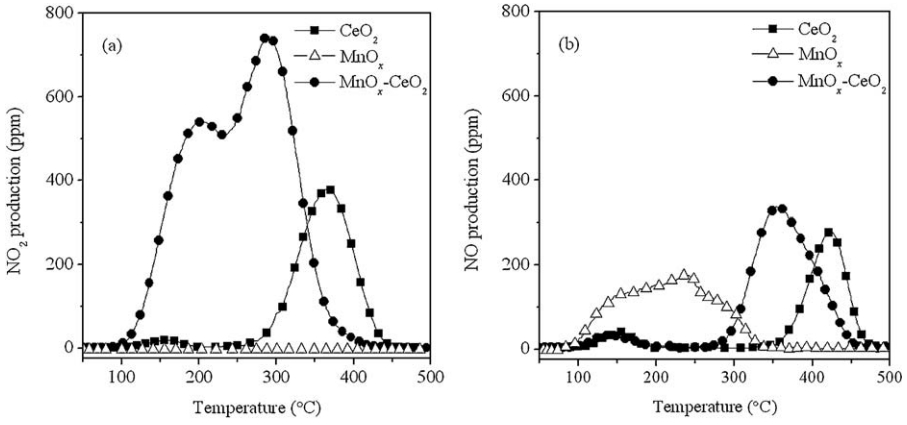

Fig. 6. (a) NO_2- and (b) NO-TPD profiles of CeO_2, MnO_x and MnO_x–CeO_2.

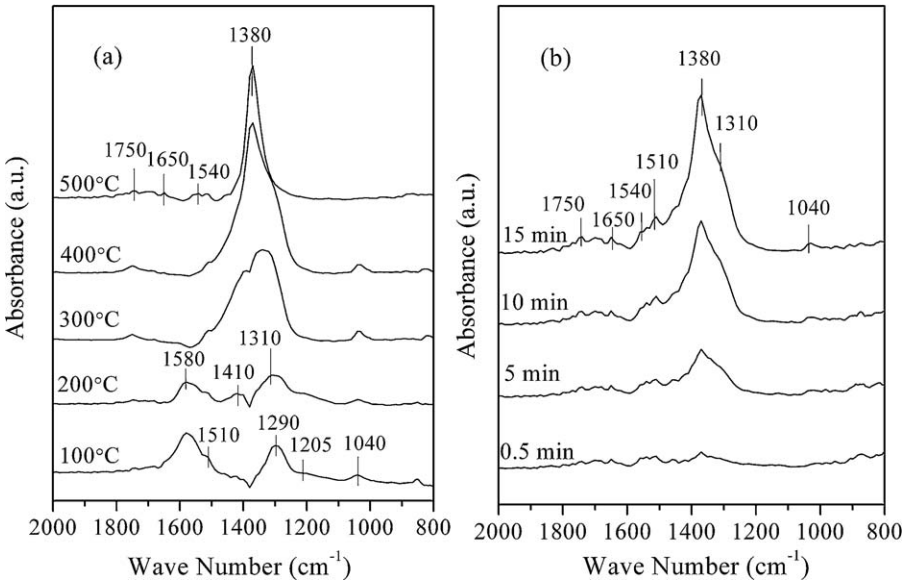

Fig. 7. DRIFTS of MnO_x–CeO_2 exposed to 1000 ppm NO/10% O_2/N_2 (a) at different temperatures and (b) at 400 °C for various time.

low temperatures (100 and 200 °C), with some other minor species such as bridging nitrates (1650 cm^{-1}), chelating nitrites (1205 cm^{-1}), nitro (1410 cm^{-1}), nitro-nitrite (1540 cm^{-1}) and N_2O_4 (1750 cm^{-1}). The bands assigned to monodentate/bidentate nitrates are gradually replaced by another band at 1380 cm^{-1}, arising from the formation of ionic nitrate at 300 °C, which correlates well with the NO_x-TPD result in Fig. 6a. Meanwhile, the chelating nitrite disappears at this temperature.

The above results indicate that NO can be oxidized readily to NO_2 on the mixed oxide catalyst in the excess O_2 and be stored mainly in the form of ionic nitrate at high temperatures. This point of view is demonstrated by the time evolution of NO_x adsorption on MnO_x–CeO_2 at 400 °C in Fig. 7b. The nitro-nitrite (1540 cm^{-1}) and dinitrogen tetraoxide (1750 cm^{-1}) reach the steady intensities immediately after the introduction of NO and O_2 (time = 0.5 min). The band assigned to ionic nitrate (1380 cm^{-1}), as well as those assigned to monodentate nitrate (1510 and 1040 cm^{-1}), bidentate nitrate (1310 and 1040 cm^{-1}) and bridging nitrate (1650 cm^{-1}), increases in intensity with the adsorption time. It indicates that the required NO_2 for soot oxidation may be mainly generated from the decomposition of ionic nitrate and monodentate/bidentate nitrates.

In order to explore possible surface intermediates formed during catalytic oxidation soot with O_2 and NO + O_2, the MnO_x–CeO_2 catalyst powders were mixed with soot particles and the soot–catalyst mixture was diluted by KBr before put into the IR cell. Similar *in situ* DRIFTS measurements with the soot–catalyst mixture have been performed recently to obtain the information of formation of surface oxygen complexes over $La_{0.9}K_{0.1}CoO_3/CeO_2$ [38], $BaAl_2O_4$ [39] and $MnO_x/Ce_{0.75}Zr_{0.25}O_2$ [40] catalysts. The spectra were recorded as a function of temperature at a heating rate of 10 °C/min. Fig. 8a shows the spectra of the soot–catalyst mixture exposed to 10% O_2/N_2 at different temperatures. The weak bands at 1460 and 1395 cm^{-1} existing during the entire temperature range are attributed to the asymmetric and symmetric stretching vibration of H–C–H of methyl [40]. The bands at 1205 and 1090 cm^{-1} are ascribed to the stretching of C–OH from hydroxyl species [41], which become less intense as the

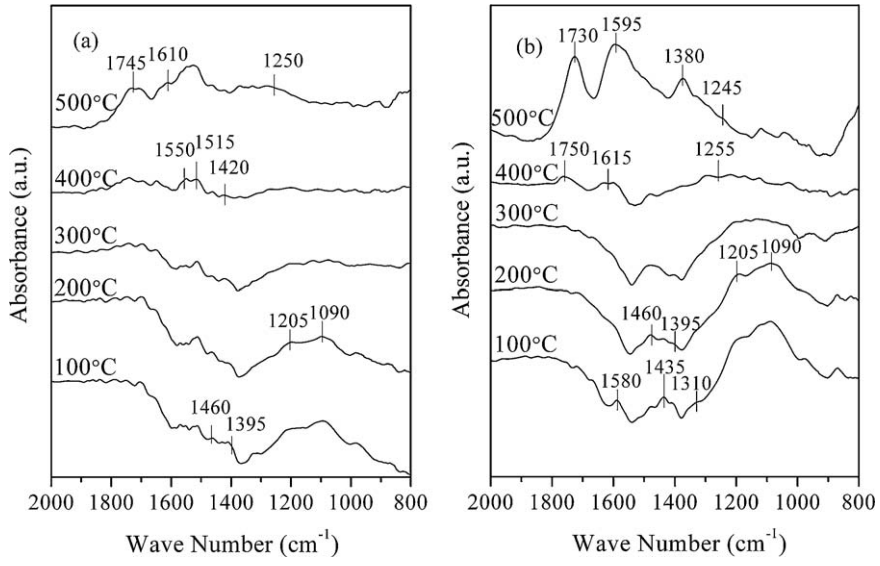

Fig. 8. DRIFTS of the soot–MnO_x–CeO_2 mixture exposed to (a) 10% O_2/N_2 and (b) 1000 ppm NO/10% O_2/N_2 at different temperatures.

temperature rises and almost disappear at 300 °C. The bands at 1550 and 1420 cm^{-1} attributed to the COO symmetric and asymmetric stretching of aromatic carboxylate species [40], as well as the band at 1515 cm^{-1} very likely assigned to some aromatic compounds, become obvious at 400 °C and reach the maxima at 500 °C. There are three other distinct bands of interest in the spectrum obtained at 500 °C: one band at 1745 cm^{-1}, associated with C=O stretching in carboxylic anhydrides and lactones, one at 1610 cm^{-1} associated with C=O stretching in quinone and ceto-enol groups, and a broad band centered at 1250 cm^{-1} associated with C–O stretching in ethers, lactones, phenols and carboxylic anhydrides [41,42].

The *in situ* DRIFT spectra of the soot–catalyst mixture exposed to 1000 ppm NO/10% O_2/N_2 were also recorded and the results are shown in Fig. 8b. Again, lots of hydroxyl species (1205 and 1090 cm^{-1}) are adsorbed on the mixed oxides and desorb at high temperatures. Methyl groups (1460 and 1395 cm^{-1}) are observed in the entire temperature range tested. The NO_x-derived adsorbates at low temperatures like bidentate nitrates (1580 and 1310 cm^{-1}), nitro compounds (1435 cm^{-1}) and/or chelating nitrite (1205 cm^{-1}) decompose or change to ionic nitrates (1380 cm^{-1}) at high temperatures. The bands assigned to surface oxygen complexes (SOCs), including carboxylic anhydrides and lactones (1750 and 1255 cm^{-1}), quinone and ceto-enol groups (1615 cm^{-1}), and ethers and phenols (1255 cm^{-1}), appear at 400 °C. These bands increase sharply in intensity and shift to lower wave numbers (1730, 1595 and 1245 cm^{-1}, respectively) at 500 °C.

On the basis of the experimental evidence described herein, as well as reports in the literatures [42,43], the soot oxidation assisted by NO_x can be divided into three steps: the formation of NO_2, the formation of SOCs, and the decomposition of SOCs. It has been found according to the NO_x-TPD results (Fig. 6) that the NO_x storage capacity of MnO_x–CeO_2 in the form of surface nitrate and nitrite is 3.3 times of ceria and 4.3 times of manganese oxide. On the other hand, both MnO_x–CeO_2 and MnO_x show good activities for catalytic oxidation of NO in excess O_2 (Fig. 5). In this way, the NO_2 can be released by decomposition of surface nitrates (Eq. (1)) and be produced by catalytic oxidation of gaseous NO (Eq. (2)) on MnO_x–CeO_2 mixed oxides in a wide temperature range.

$$NO_3^- \leftrightarrow O_2 + NO_2 \quad (1)$$

$$NO + O^*_{Catal} \leftrightarrow NO_2 \quad (2)$$

These NO_2 species, nitrate- and NO-derived NO_2, contribute to the oxidation of soot importantly. Soot oxidation can be initiated by the reaction between carbon surface species (C_s) and NO_2 (Eq. (3)):

$$C_s + NO_2 \leftrightarrow C(O) + NO \quad (3)$$

$$C_s + O^*_{Catal} \rightarrow C(O) \quad (4)$$

where surface oxygen complexes C(O) are formed. The bands at 1750–1730, 1615–1595 and 1255–1245 cm^{-1} appear at 400 °C and becomes strong at 500 °C in NO + O_2 (Fig. 8b), suggesting the generation of carboxylic anhydrides, lactones, quinine, ceto-enol groups, ethers and phenols as important SOCs. They can be also produced by the oxidation of soot with active oxygen from the catalyst (Eq. (4)), although the onset temperature is raised to a relatively higher temperature (500 °C as shown in Fig. 8a). Due to different soot–catalyst–gas contact conditions, the effect of NO_2 on soot oxidation in the DRIFTS experiment is expected to be less efficient than that exhibited in the soot-TPO test, leading to the delayed onset temperatures.

The SOCs decomposition by releasing CO_2 and/or forming low-carbon surface species C'_s can occur through thermal dissociation of intermediates (Eq. (5)) or through the reactions with O_2 (Eq. (6)) and NO_2 (Eq. (7)). Reaction (6) is assumed predominant due to the abundance of gaseous oxygen. However, these aspects need to be further clarified and investigation is presently ongoing in our lab.

$$C(O) \rightarrow CO_2(+C'_s) \quad (5)$$

$$C(O) + O_2 \rightarrow CO_2(+C'_s) \quad (6)$$

$$C(O) + NO_2 \rightarrow NO + CO_2 + (+C'_s) \quad (7)$$

4. Conclusions

In respect to the individual oxides MnO_x and CeO_2, the MnO_x–CeO_2 mixed oxide catalyst exhibits a lower ignition temperature and maximal oxidation rate temperature in the presence of 1000 ppm NO and 10% O_2. This catalyst in the form of solid solutions reveals small crystallite size, large surface area and superior low-temperature redox property. Especially, the high NO oxidation activity and high NO_2 storage capacity are two main factors to make MnO_x–CeO_2 mixed oxides as a suitable candidate for NO_x-assisted soot oxidation. NO_2 generated from catalytic oxidation of NO and decomposition of surface nitrates reacts with soot and creates surface oxygen complexes like carboxylic anhydrides, lactones, quinine, ceto-enol groups, ethers and phenols, which occurs at about 100 °C lower temperature than the case without NO in the *in situ* DRIFTS tests and is believed to be the most important step for soot oxidation.

Acknowledgements

The authors would like to acknowledge Projects 2010CB732304 and 2009AA064801 supported by the Ministry of Science and Technology of China.

References

[1] D.M. Brown, M.R. Wilson, W. MacNee, V. Stone, K. Donaldson, Toxicol. Appl. Pharm. 175 (2001) 191.
[2] D. Fino, N. Russo, G. Saracco, V. Specchia, J. Catal. 242 (2006) 38.
[3] R. Allanson, B.J. Cooper, J.E. Thoss, A. Uusimäki, A.P. Walker, J.P. Warren, SAE Paper No. 2000-01-0480 (2000).
[4] K. Yoshida, S. Makino, S. Sumiya, G. Muramatsu, R. Helferich, SAE Paper No. 892046 (1989).
[5] B.J. Cooper, J.E. Thoss, SAE Paper No. 890404 (1989).
[6] Y. Teraoka, K. Nakano, W.F. Shangguan, S. Kagawa, Catal. Today 27 (1996) 107.
[7] Q. Li, M. Meng, Z.Q. Zou, X.G. Li, Y.Q. Zha, J. Hazard. Mater. 161 (2009) 366.
[8] J. Liu, Z. Zhao, C.M. Xu, A.J. Duan, G.Y. Jiang, J. Phys. Chem. C 112 (2008) 5930.
[9] R. Matarrese, L. Castoldi, L. Lietti, P. Forzatti, Top. Catal. 42 (2007) 293.
[10] A. Setiabudi, M. Makkee, J.A. Moulijn, Top. Catal. 30 (2004) 305.
[11] R.S. Zhu, M.X. Guo, F. Ouyang, Catal. Today 139 (2008) 146.
[12] Y. Teraoka, K. Kanada, S. Kagawa, Appl. Catal. B 34 (2001) 73.
[13] R. Lopez-Fonseca, U. Elizundia, I. Landa, M.A. Gutierrez-Ortiz, J.R. Gonzalez-Velasco, Appl. Catal. B 61 (2005) 150.
[14] X.D. Wu, Q. Liang, D. Weng, Z.X. Lu, Catal. Commun. 8 (2007) 2110.
[15] Z.P. Wang, Z. Jiang, W.F. Shangguan, Catal. Commun. 8 (2007) 1659.
[16] F.E. López-Suárez, A. Bueno- López, M.J. Illán-Gómez, A. Adamski, B. Ura, J. Trawczynski, Environ. Sci. Technol. 42 (2008) 7670.
[17] F.E. López-Suárez, S. Parres-Esclapez, A. Bueno-López, M.J. Illán-Gómez, B. Ura, J. Trawczynski, Appl. Catal. B 93 (2009) 82.
[18] I. Atribak, A. Bueno-López, A. García-García, P. Navarro, D. Frías, M. Montes, Appl. Catal. B 93 (2010) 267.
[19] A. Bueno-López, K. Krishna, M. Makkee, J.A. Moulijn, J. Catal. 230 (2005) 237.
[20] E. Aneggi, C. de Leitenburg, G. Dolcetti, A. Trovarelli, Catal. Today 114 (2006) 40.
[21] A. Setiabudi, J. Chen, G. Mul, M. Makkee, J.A. Moulijn, Appl. Catal. B 51 (2004) 9.
[22] M. Machida, Y. Murata, K. Kishikawa, D.J. Zhang, K. Ikeue, Chem. Mater. 20 (2008) 4489.
[23] K. Tikhomirov, O. Kröcher, M. Elsener, A. Wokaun, Appl. Catal. B 64 (2006) 72.
[24] M. Machida, M. Uto, D. Kurogi, T. Kijima, Chem. Mater. 12 (2000) 3158.
[25] G. Zhou, P.R. Shah, R.J. Gorte, Catal. Lett. 120 (2008) 191.
[26] G. Qi, R.T. Yang, J. Phys. Chem. B 108 (2004) 15738.
[27] M.A. Peralta, M.S. Gross, B.S. Sánchez, C.A. Querini, Chem. Eng. J. 152 (2009) 234.
[28] M.A. Peralta, M.S. Gross, M.A. Ulla, C.A. Querini, Appl. Catal. A 367 (2009) 59.
[29] F. Giordano, A. Trovarelli, C.D. Leitenburg, M. Giona, J. Catal. 193 (2000) 273.
[30] Q. Liang, X.D. Wu, D. Weng, H.B. Xu, Catal. Today 139 (2008) 113.
[31] E. Aneggi, C. del Leitenburg, G. Dolcetti, A. Trovarelli, Catal. Today 114 (2006) 40.
[32] Q. Liang, X.D. Wu, X.D. Wu, D. Weng, Catal. Lett. 119 (2007) 265.

[33] I. Atribak, B. Azambre, A. Bueno López, A. García-García, Appl. Catal. B 92 (2009) 126.
[34] M. Machida, M. Uto, D. Kurogi, T. Kijima, J. Mater. Chem. 11 (2001) 900.
[35] K.I. Hadjiivanov, Catal. Rev. Sci. Eng. 42 (2000) 71.
[36] G. Qi, R.T. Yang, R. Chang, Appl. Catal. B 51 (2004) 93.
[37] A.L. Kustov, M. Makkee, Appl. Catal. B 88 (2009) 263.
[38] J. Liu, Z. Zhao, J. Lan, C.M. Xu, A.J. Duan, G.Y. Jiang, X.P. Wang, H. He, J. Phys. Chem. C 113 (2009) 17114.
[39] H. Lin, Y.J. Li, W.F. Shangguan, Z. Huang, Combust. Flame 156 (2009) 2063.
[40] V.S. Escribano, E.F. López, J.M. Gallardo-Amores, C. del, H. Martínez, C. Pistarino, M. Panizza, C. Resini, G. Busca, Combust. Flame 153 (2008) 97.
[41] J.L. Figueiredo, M.F.R. Pereira, M.M.A. Freitas, J.J.M. Órfão, Carbon 37 (1999) 1379.
[42] A. Setiabudi, M. Makkee, J.A. Moulijn, Appl. Catal. B 50 (2004) 185.
[43] W.J. Zhang, S. Rabiei, A. Bagreev, M.S. Zhuang, F. Rasouli, Appl. Catal. B 83 (2008) 63.